G. Panzarasa, A. Osypova, J. Ribera, F.W. M. R. Schwarze, F. Quasso, G. Consolati
Hybrid Adsorbent Materials Obtained by the Combination of Poly(ethylene-alt-maleic anhydride) with Lignin and Lignosulfonate
Journal of Polymers and the Environment, Vol. 26, N. 11, 2018, p. 4293-4302
doi:10.1007/s10924-018-1299-z

Hybrid Adsorbent Materials Obtained by the Combination of Poly(ethylene-*alt*-maleic anhydride) with Lignin and Lignosulfonate

Guido Panzarasa[1,6], Alina Osypova[2,7], Javier Ribera[3] ·, Francis W. M. R. Schwarze[3] ·, Fiorenza Quasso[4] ·, Giovanni Consolati[4,5]

1. Department of Polymer Engineering and Science, Montanuniversität, Otto-Glöckel Straβe 2, 8700 Leoben, Austria
2. Sorbonne Universités, UPMC Univ Paris 06, 75005 Paris, France
3. Empa Materials Science and Technology, Laboratory for Applied Wood Materials, Lerchenfeldstrasse 5, 9014 St. Gallen, Switzerland
4. Department of Aerospace Science and Technology, Politecnico di Milano, via La Masa 34, 20156 Milano, Italy
5. INFN, sezione di Milano, via Celoria 16, 20133 Milano, Italy
6. Present Address: Laboratory for Soft and Living Materials, Department of Materials, ETH Zürich, Vladimir-Prelog-Weg 5, 8093 Zurich, Switzerland
7. Present Address: Innovative Sensor Technology IST AG, Stegrütistrasse 14, 9462 Ebnat-Kappel, Switzerland

Abstract

Lignin is one of the most available biomass products, but its potential for the development of functional materials has yet to be unleashed. Here, the modification of lignin and lignosulfonate with poly(ethylene-*alt*-maleic anhydride) [P(E-*alt*- MA)], a functional polymer of wide industrial use, is accomplished by means of a simple esterification reaction. As a result, hybrid adsorbent materials for water purification can be obtained, which were thoroughly characterized. The combination of P(E-*alt*-MA) with lignin increased hydrophilicity of the latter, making it dispersible in aqueous environments, while with lignosulfonate it gave rise to a water-insoluble, thus easily recoverable, product. The adsorption properties of the resulting products have been tested against a model water pollutant (methylene blue), demonstrating remarkable adsorption speed (in the order of minutes), adsorption efficiency and stability over a wide range of pH (2–12). Moreover, after the incorporation of magnetite nanoparticles by in situ synthesis, adsorbent materials able to be magnetically recovered were developed.

Keywords Lignin · Lignosulfonate · Poly(ethylene-*alt*-maleic anhydride) · Adsorbent materials · Water purification

Introduction

Functional materials obtained from renewable sources, such as organic biomass, hold the promise to allow a sustainable transition towards "greener" processes and products [1, 2]. In this framework, natural biopolymers (cellulose, lignin, chitin, chitosan, alginate and agarose, to name a few) represent one of the most interesting playground thanks to their wide availability and rich variety of physico-chemical properties [3]. Lignin is a structural material in wood and is the second most abundant terrestrial polymer after cellulose. It has a complex chemical structure, consisting of three monomers: p-coumaryl, coniferyl and sinapyl alcohols (the relative ratios of whose can vary depending on the plant species), linked together by highly branched methoxylated phenyl-propane units (Scheme S1) [4,5]. Thanks to the presence of phenolic and hydroxyl groups it is possible to chemically modify lignin in a variety of ways, using a range of relatively simple chemistries, resulting in high-value polymeric products and materials [6-10]. This explains the great

interest, both academic and industrial, in the chemistry of lignin. In the so-called sulfite process, lignin (or directly wood chips) is cooked in presence of sulfites: the sulfonation of the α-carbon atoms of lignin then results in lignosulfonates, anionic polyelectrolytes with wide industrial applications, e.g. as dispersing agents [11].

Despite its great interest for biomass valorization processes, however, lignin is still an underutilized feedstock for the development of functional materials. In this context, the development of novel adsorbent materials for water treatment is a rapidly-evolving field, due to the increasing demand of drinkable water [12, 13]. For the removal of contaminants from wastewater, methods based on adsorp- tion are usually preferable compared to those based e.g. on precipitation, as they are more versatile and allow for easier management of the resulting spent materials. It is crucial, then, to develop efficient and sustainable adsorbent materials, as well as to ensure that the spent adsorbents could be disposed of without generating additional waste [14]. The production of materials and composites derived from natural and renewable sources has a special relevance to facilitate the meeting of this requirements, an approach which has its roots in biomass valorization [15].

In a recent publication [16] we reported a convenient synthetic protocol to prepare an adsorbent material by the combination of sepia melanin and poly(ethylene-alt-maleic anhydride) [P(E-alt-MA)], a widely used industrial polymer. The resulting hybrid displayed a remarkable stability as well as a high efficiency towards to the adsorption of methylene blue (MB) from aqueous solutions over a wide pH range (2-12) and in high ionic strength conditions. Here, we want to demonstrate the versatility of our method by applying it to different kinds of biopolymers, lignin and lignosulfonate. The resulting hybrid products have been fully characterized by means of different techniques and their adsorption properties tested for MB. Moreover, we demonstrate that the hybrids are easily functionalized with magnetite nanoparticles, allowing their recovery by means of a magnet.

Materials and Methods

Lignin (alkali, avg. $M_w \sim 28{,}000$ g mol^{-1}, avg. $M_n \sim 5000$ g mol^{-1}), sodium lignosulfonate (avg. $M_w \sim 52{,}000$ g mol^{-1}, avg. $M_n \sim 7000$ g mol^{-1}), poly(ethylene-*alt*-maleic anhydride) [P(E-*alt*-MA), M = 100,000–500,000 g mol^{-1}], 1-methylimidazole (≥ 99%, purified by redistillation), 1,4-dioxane (≥ 99%), ethanol (anhydrous), iron(II) and iron(III) chloride, concentrated ammonium hydroxide (28%, ACS reagent), concentrated sulfuric acid (95–98%), concentrated hydro-chloric acid (32%), sodium hydroxide and MB, were purchased from Sigma-Aldrich (ACS reagent grade) and used as received. Water obtained from a MilliQ purification system was used.

Physico-Chemical Characterization Techniques

Fourier transform infrared spectroscopy (FTIR) was performed using a Nicolet™ iN™10 equipped with a liquid nitrogen-cooled MCT detector (spectral range 4000–700 cm^{-1}, resolution 4 cm^{-1}); background (500 scans) was collected before each sample (1000 scans). UV–Vis absorption spectra were obtained using a Genesys 10S UV–Visible spectrophotometer. Scanning electron microscopy (SEM) and energy dispersive X-ray spectroscopy (EDX) were carried out using a Hitachi S-4800 scanning electron microscope equipped with an INCA X-Sight EDS (Oxford Instruments) detector. The samples were fixed on conductive carbon tape and sputter- coated with 5 nm of Au/Pd alloy to facilitate imaging. EDX was performed with an acceleration voltage of 10 kV and semi-quantitative elemental analysis data were obtained using the ZAF approach. Thermogravimetric analysis (TGA) was performed with a Netzsch TG 209 F1 Iris instrument on 5 mg-samples in alumina crucibles under a nitrogen atmosphere (flow rate 25 mL min^{-1}), scanning a temperature range from 25 °C to 900 °C with a heating rate of 10 °C min^{-1}. Differential scanning calorimetry (DSC) measurements were carried out by means of a Mettler Toledo DSC 822e instrument calibrated with high purity standards (indium and zinc). Samples of 3.5–5 mg were encapsulated in aluminum pans and heated from 20 to 250 °C at a rate of 10 °C min^{-1} under nitrogen flux. For each sample, two heating and cooling cycles were performed. The glass transition temperature (T_g) was obtained as the inflection point of the heat capacity increment associated with the glass-to-rubber transition. The melting temperature was determined as the peak value of the endothermic phenomenon. The melting enthalpy per unit mass (ΔH_m) was calculated from the area under the corresponding endothermic peak.

Synthesis of the Adsorbent Materials: Lignin-P(E-*alt*-MA) and Lignosulfonate-P(E-*alt*-MA)

In a 250 mL three-necked round-bottomed flask, equipped with a condenser, 2.5 g of poly(ethylene-*alt*-maleic anhydride) were dissolved in a mixture of 30 mL of 1-methylimidazole and 15 mL of dioxane under stirring. Then, 2.5 g of lignin (or sodium lignosulfonate) were suspended in 85 mL dioxane and added to the solution in the flask. The mixture was refluxed at 100 °C under stirring for 2 h and then allowed to cool to room temperature. The supernatant was discarded and water was added directly to break the precipitate forming a loose gel, which was collected by centrifugation and washed repeatedly with water until the washings were colorless. Then, the solid was resuspended in 300 mL of water under stirring overnight to complete the washing. Eventually, the solid was dehydrated with ethanol to obtain a fine powder which was dried under vacuum overnight. The yield was 3.7 ± 0.1 g (74%, on mass basis) for lignin-P(E-*alt*-MA) and 3.25 ± 0.2 g (65%, on mass basis) for lignosulfonate-P(E-*alt*-MA). Lyophilization was also performed on rehydrated samples.

Functionalization of Lignin-P(E-*alt*-MA) and Lignosulfonate-P(E-*alt*-MA) with Magnetite Nanoparticles to Obtain Magnetically-Separable Hybrids

In a glass vial, 20 mg of lignin-P(E-*alt*-MA) or lignosulfonate-P(E-*alt*-MA) were stirred (15 min, 250 rpm, 25 °C) with 5.5 mL of a solution containing 73 mM $FeCl_3$ and 36 mM $FeCl_2$ (molar ratio $Fe^{3+}/Fe^{2+} = 2$) in 0.2 M HCl to promote the uptake of the metal cations [17]. Then, under stirring, 5 mL of concentrated NH_4OH were added to generate the magnetite nanoparticles. The resulting composites were freed by the excess reagents and non-attached magnetite particles by cycles of centrifugation and redispersion in water. The composites were readily attracted by a magnet. The composites were then lyophilized and analyzed by means of SEM and EDX.

Adsorption Studies

Effect of pH on Adsorption Efficiency

The effect of pH on the adsorption efficiency was studied using a 1 g L^{-1} amount of adsorbent. Solutions with controlled pH values ranging from 2 to 12 were prepared by adjusting the pH of a phosphate buffer (PB), containing 50 mg L^{-1} of MB, with 1 M HCl and 1 M NaOH solutions. Each solution was mixed with the adsorbent material for 30 min under orbital shaking (250 rpm) at 25 °C. The solutions were then filtered through a 0.45 µm PTFE syringe filter, their UV–Vis spectra were measured in the range 400–900 nm and their absorbance at 644 nm was recorded. The adsorption efficiency *AE %* was calculated according to Eq. (1):

$$AE\% = \frac{Abs0 - Abs}{Abs0} \times 100 \quad (1)$$

where Abs_0 and *Abs* are, respectively, the initial absorbance and the absorbance after treatment, measured at 664 nm.

Effect of Adsorbent Dosage

The effect of adsorbent dosage on the adsorption efficiency was studied using 0.125, 0.25, 0.5, 1 and 2 g L^{-1} amounts of adsorbent. The experiments were done at pH 4 using the PB solution containing 50 mg L^{-1} of MB. The same procedure described previously was followed.

Effect of Adsorption Time

The effect of adsorption time on the adsorption efficiency was studied in a time interval from 5 min to 60 min. The experiments were conducted at pH 4 using the PB solution containing 50 mg L^{-1} of MB. The same procedure described previously was followed.

Results and Discussion

Alternating polymers made by the copolymerization of maleic anhydride with different alkenes, have been described since the mid-1940s broad use in the petroleum, textile and cosmetic industry as dispersing agents, emulsion stabilizers, surfactants, viscosity modifiers and compatibilizers for polymer blends [18]. Such a variety of applications is made possible by the intrinsically rich palette of properties exhibited by these polymers. The nature of the alkene co-monomer dictates the relative hydrophobicity, solubility and assembly properties, while the anhydride moieties can react with different functional groups, including alcohols, amines and thiols (Scheme S2). In an alkaline environment, the anhydride converts to a dicarboxylate and the polymer is transformed to an anionic polyelectrolyte. Here, we made P(E-*alt*-MA) to react with lignin and lignosulfonate. The reaction, in its essence, is an esterification as depicted in Scheme 1a. As a reaction medium, we found a 1:2 v/v mixture of dioxane and 1-methylimida- zole to be a favorable one, thanks to the combined solvent properties and the catalytic activity of 1-methylimidazole for promoting the esterification reaction (Scheme 1b) [19]. After the reaction, the products could be easily recovered by precipitation with water, by washing dehydration with ethanol. The treatment with ethanol is helpful not only to ensure the removal of reaction by-products and solvents but also to convert otherwise swollen, gel-like materials to easy- to-handle powders (Fig. S1).

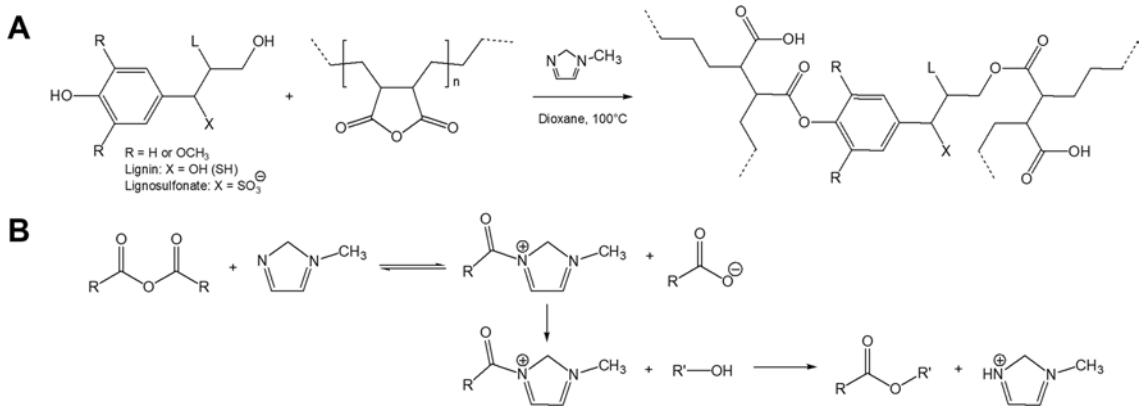

a Reaction scheme for the esterification of lignin and lignosulfonate with P(E-*alt*-MA). The letter "L" and the dashed lines both indicate the continuation of the molecular structure. **b** Reaction scheme for a 1-methylimidazole-catalyzed esterification reaction between an alcohol group and a generic anhydride [19]. First the anhydride reacts with the 1-methylimidazole generating a *N*-alkyl-*N*'-methylimidazolium ion, then reacts irreversibly with the –OH group. The 1-methylimidazole acts also as a proton scavenger. R and R′ can be any aliphatic or aromatic group

As a first proof for successful reaction, it was observed that both the lignin-P(E-*alt*-MA) and lignosulfonate-P(E- *alt*-MA) hybrids were insoluble in alkaline solutions, even in concentrated (5 M) aqueous sodium hydroxide. Such a result strongly suggested that the desired molecular change had taken place sinceP(E-*alt*-MA) was especially soluble at basic pH due to the conversion of anhydride groups into carboxylates. Most importantly, when a control reaction was run in the same conditions using only P(E-*alt*-MA), a small amount of a white gelatinous product could be obtained, which readily and completely dissolved in 5 M NaOH. To better understand the molecular structure of the hybrid products, the synthesis of succynilated lignin and succynilated lignosulfonate was also performed. A detailed description of their synthesis and of their characteristics can be found in the Supporting Information (Figs. S5–S7).

Morphology and Chemical Composition Analysis

The morphology of both starting and synthesized materials was investigated by means of SEM. The results are shown in Fig. 1. The raw lignin and lignosulfonate appeared as poly-disperse microparticles, some of which were spheroidal and most of them hollow (Fig. 1a, d). The observed morphology is compatible with their production by means of spray drying [11]. The most striking change in morphology was observed for the lignin-P(E-*alt*-MA) hybrid (Fig. 1b), which showed porous, quasi-fractal aggregates. However, no appreciable differences could be observed after lyophilization

(Fig. 1c). The lignosulfonate-P(E-*alt*-MA) hybrid showed aless porous structure and larger aggregates (Fig. 1e). After lyophilization, they gave rise to an interconnected network (Fig. 1f).
The SEM morphology of the magnetite nanoparticles-functionalized hybrids is shown in Fig.2. Magnetite nanoparticles were visible as small spheres (Fig. 2b, e), which were absent in the images, taken at the same magnification, of unmodified hybrids (Fig. 2c, f).
Energy-dispersive X-ray (EDX) spectroscopy provided a semi-quantitative elemental composition for all the investigated materials. The results for raw lignin and lignosulfonate were in good agreement with literature values, considering the unavoidable variability due to different sources and production methods [4]. EDX allowed us also to demonstrate the successful incorporation of magnetite nanoparticles. According to the C/Fe ratios, the functionalization pro- cess was more efficient for the lignosulfonate-P(E-*alt*-MA) hybrid, a result which can be conveniently explained by the presence of sulfonate groups with strong affinity for iron ions. The complete EDX spectra is shown in Fig. S2 and S3, while the results are summarized in Table 1.

Thermal Analysis

The thermal properties of the precursors and of the synthesized materials were tested by means of DSC and TGA. The DSC profile of poly(E-*alt*-MA) showed only an endothermic peak at 145 °C due to melting (the associated enthalpy being ΔH_m = 2.6 J g^{-1}), no glass transition temperature could be observed. On the other hand, glass transition temperatures could be measured for lignin and lignosulfonate, the corresponding T_g values being 174 °C and 85 °C, respectively. The T_g found for lignin is in excel- lent agreement with literature values [8,10,20], while the T_g of lignosulfonate is consistently lower compared to literature values: for example, Jiang et al. [20] reported T_g values of 127 °C for hardwood-derived lignosulfonate and 138 °C for softwood-derived lignosulfonate. Such difference could be due to different factors, including: different molecular characteristics (molecular mass distribution, concentration of functional groups and branches); different water content (lignosulfonates are hydrophilic and tend to absorb humid- ity from air, with a consequent decrease in T_g [10]); different measurement conditions (*e.g.* heating rate) and different evaluation methods (T_g could be obtained from the inflection point of the heat capacity increment, as in our case, or from the peak of heat capacity change). Nevertheless, a strong lowering of T_g was observed for both synthesized materials, lignin-P(E-*alt*-MA) and lignosulfonate-P(E-*alt*-MA), with values of 52 °C and 45 °C respectively. This suggests a strong interaction between the lignin (and lignosulfonate) and poly(E-*alt*-MA). Grafting of poly(ethylene) chains to lignin and lignosulfonate loosens the rigid matrix, thus its segmental motion can be initiated at lower temperatures. As a result, the glass transition decreases. The DSC plots are shown in Fig. S4.
The TGA plots are shown in Fig.3 along with their corresponding differential thermal analysis (DTA) plots. Poly(ethylene-*alt*-maleic anhydride) (inset in the DTA graphs) showed three distinct mass losses: a weak one at 150 °C (water elimination) and two more intense at 311 °C and at 430 °C (polymer decomposition). In the case of lignin, two mass losses were visible: one at 60 °C (water desorption) and the other, broader, with a maxi- mum at 360 °C (lignin decomposition) [21]. For the lignin-P(E-*alt*-MA), apart from the water loss at 59 °C, a new unidentified mass loss appeared at 180 °C, prob- ably due to water elimination, while the losses at 329 °C and 397 °C can be explained by lignin decomposition and P(E-*alt*-MA) decomposition, respectively. In the case of lignosulfonate, the mass loss at 90 °C can be attributed to water desorption while a broad mass loss with two peak at 259 °C and 289 °C can be attributed to the decom- position of lignosulfonate [22].
For the lignosulfonate- P(E-*alt*-MA), water loss occurred at 70 °C, followed by a sequence of three increasing weight losses, at 210 °C, 329 °C and 446 °C, that can be attributed respectively to lignosulfonate decomposition and P(E-*alt*-MA) decomposition. The residual mass percentages at 900 °C (Table2) allowed to estimate the amount of P(E-*alt*-MA) combined with lignin and lignosulfonate in the synthesized materials, about 37 wt% and 70 wt%, respectively (see the Supporting Information for details about the calculations) The residues for all the substances tested appeared of carbonaceous nature, as expected from the use of an inert (non-oxidizing) atmosphere to carry out TGA and in accordance with previous literature results for lignin and lignosulfonate [23]

Fourier-Transform Infrared Spectroscopy (FTIR)

The changes in the chemical structure of lignin and lignosulfonate after the esterification with P(E-*alt*-MA) are apparent in the FTIR spectra (Fig.4). The assignment of the FTIR peaks was based on the existing literature [24–

26]. For poly(ethylene-*alt*-maleic anhydride), the intense peak at 1775 cm^{-1} is characteristic for the stretching of the C=O bonds. The absorbances at 2930 cm^{-1} and 2870 cm^{-1} are related to the asymmetric and symmetric stretching vibrations of C–H in CH_2 groups.

For lignin and lignosulfonate, the broad absorption at 3400 cm^{-1} was attributed to the stretching vibration of O–H and the weak peaks centered at around 2930 cm^{-1} and 2850 cm^{-1} were assigned to the asymmetric and symmetric stretching vibrations of C–H in CH_3 and CH_2 groups, respectively. The peaks corresponding to the aromatic C=C skeletal vibrations were visible at 1608 cm^{-1} (quinoid), 1510 cm^{-1} and 1425 cm^{-1}. The peak at 1460 cm^{-1} was attributed to the deformation vibration of C–H in both CH_3 and CH_2 groups. The peak at 1032 cm^{-1}, especially intense for lignosulfonate, is associated to the stretching of C–S. The spectrum of lignin was more detailed compared to that of lignosulfonate in the region around 1260 cm^{-1}–1060 cm^{-1}, where a peak at 1117 cm^{-1} was assigned to the in-plane deformation vibration of C–H in aromatic rings. The absorption at 630 cm^{-1}, visible only in the spectrum of lignosulfonate, is characteristic for the sulfonate group.

The appearance of a sharp peak centered at 1717 cm^{-1} and 1706 cm^{-1}, respectively in the spectra of lignin-P(E-*alt*-MA) and lignosulfonate-P(E-*alt*-MA) hybrids, can be attrib- uted to the stretching of C=O groups, which is evidence of esterification. This conclusion is supported by the results of Thielemans and Wool [19] and of Xiao et al. [27] on the esterification of lignin with cyclic anhydrides and those of Wang et al. [28] on the esterification of lignosulfonate with maleic anhydride, which also indicate that esterification takes place on the aliphatic hydroxyl groups. Nevertheless, the appearance of a peak, at 1771 cm^{-1} for lignin-P(E-*alt*- MA) and at 1774 cm^{-1} for lignosulfonate-P(E-*alt*-MA), which can be attributed to phenyl esters, suggests that a certain amount of phenolic groups has been subjected to esterification as well. The intensity of the absorption peaks in the aliphatics region also intensified compared to unmodified lignin and lignosulfonate, consistently with the presence of additional CH_2 moieties from P(E-*alt*-MA).

Evaluation of Adsorption Efficiency Towards Methylene Blue

To evaluate the potential of our synthesized hybrids as efficient adsorbent materials, MB was selected. Its solubility in water, good chemical stability over a wide range of pH and wide industrial use make MB an excellent model water pollutant. As is shown in Fig. 5a, the lignin-P(E-*alt*-MA) hybrid reached the maximum efficiency of adsorption for MB at pH 7. This is in good agreement with the reported pK_a of hydrolyzed P(E-*alt*-MA), which is around 3.65 [29]. For $pH \geq pK_a$, the carboxylic acid groups in hydrolyzed P(E-*alt*-MA) are supposed to be completely deprotonated and negatively charged, maximizing the interaction with the positively charged MB. However, the lignosulfonate- P(E-*alt*-MA) hybrid was completely active already at pH 3, most probably thanks to the sulfonate groups ($pK_a < 2$). As shown in Fig. 5b, a 0.5 g L^{-1} concentration of both hybrids is enough to ensure complete MB absorption. Moreover, our hybrids are very rapid adsorbents, reaching the peak effi- ciency after only 5 min for lignin-P(E-*alt*-MA) and almost immediately for lignosulfonate-P(E-*alt*-MA) (Fig. 5c).

Compared to pristine lignin, the lignin-P(E-*alt*-MA) hybrid is more hydrophilic, which facilitates interactions in aqueous environments. Moreover, the presence of free carboxylic groups from P(E-*alt*-MA) results in a dramatic increase of its adsorption properties for cationic species. Its superior adsorption efficiency was demonstrated by comparing its performance with that of pristine lignin and of succynilated lignin. The adsorption efficiency *AE%* was determined for all samples under the same conditions (pH 7, 1 g L^{-1} of adsorbent, 50 mg L^{-1} of MB, adsorption time 30 min, 250 rpm, 25 °C). The absorption results were 13% for lignin and 42% for succynilated lignin, while for lignin-P(E-*alt*-MA) *AE%* was 100%. The same comparison between the lignosulfonate-P(E-*alt*-MA) (which also showed an excellent performance, *AE%* being 100%), lignosulfonate and succynilated lignosulfonate could not be carried out because of the high solubility in water of the latter two. This directly points out the main drawback for the direct use of lignosulfonate and P(E-*alt*-MA) for water purification, namely the necessity of dedicated separation systems (*e.g.* membrane filtration [30]), while for the lignin and lignosulfonate hybrids simple filtration, centrifugation or even decantation is sufficient to separate them from the treated water. In the case of magnetite nanoparticle-deco- rated hybrids, the possibility to use magnetic decantation is clearly an added value (Fig. 5d).

Conclusion

As a result of our attempts to investigate new ways for the development of novel functional materials based on a combination of natural and artificial polymers, we described here a simple way to combine lignin and lignosulfonate, two

widely available and renewable biopolymers, with poly(ethylene- *alt*-maleic anhydride), a well-known industrial polymer, by means of an esterification reaction. The resulting products displayed excellent properties as adsorbent materials for water purification. The main advantages offered by the synthesized hybrids, compared to the raw materials, are complete (> 99%) and rapid (in the order of minutes) adsorption efficiency for cationic species (MB) at a wide range of pH (2–12), coupled with remarkable stability and insolubility. Functionalization of hybrids with magnetite nanoparticles results in composites which are easily attracted by a magnet, thus making their recovery easily accomplishable.

References

1. Eichhorn SJ, Gandini A (2010) Materials from renewable resources. MRS Bull 35:187–193. https://doi.org/10.1557/mrs2010.650
2. Kim HC, Mun S, Ko HU et al (2016) Renewable smart materials. Smart Mater Struct 25:073001
3. Schnepp Z (2013) Biopolymers as a flexible resource for nanochemistry. Angew Chem Int Ed 52:1096–1108
4. Chung H, Washburn NR (2015) Extraction and types of lignin. In: Omar F, Mohini S (eds) Lignin in polymer composites. William Andrew, New York, pp 13–25
5. Gargulak JD, Lebo SE Jr, McNally TJ (2001) Lignin. In: Kroschwitz JI (ed) Kirk-Othmer encyclopedia of chemical technology, 4th edn. Wiley, New York
6. Duval A, Lawoko M (2014) A review on lignin-based polymeric, micro- and nano-structured materials. React Funct Polym 85:78–96. https://doi.org/10.1016/j.reactfunctpolym.2014.09.017
7. Laurichesse S, Avérous L (2014) Chemical modification of lignins: towards biobased polymers. Prog Polym Sci 39:1266–1290
8. Doherty WOS, Mousavioun P, Fellows CM (2011) Value-adding to cellulosic ethanol: lignin polymers. Ind Crops Prod 33:259–276
9. Upton BM, Kasko AM (2016) Strategies for the conversion of lignin to high-value polymeric materials: review and perspective. Chem Rev 116:2275–2306
10. Kun D, Pukánszky B (2017) Polymer/lignin blends: interactions, properties, applications. Eur Polym J 93:618–641
11. Aro T, Fatehi P (2017) Production and application of lignosulfonates and sulfonated lignin. ChemSusChem 10:1861–1877
12. Schwarzenbach RP, Egli T, Hofstetter TB et al (2010) Global water pollution and human health. Annu Rev Environ Resour 35:109–136. https://doi.org/10.1146/annurev-environ-100809-125342
13. Wang Q, Yang Z (2016) Industrial water pollution, water environment treatment, and health risks in China. Environ Pollut 218:358–365. https://doi.org/10.1016/j.envpol.2016.07.011
14. Shannon M, Bohn PW, Elimelech M et al (2008) Science and technology for water purification in the coming decades. Nature 452:301–310. https://doi.org/10.1038/nature06599
15. Tuck CO, Pérez E, Horváth IT et al (2012) Valorization of biomass: deriving more value from waste. Science 337:695–699
16. Panzarasa G, Osypova A, Consolati G et al (2018) Preparation of a sepia melanin and poly (ethylene-alt-maleic anhydride) hybrid material as an adsorbent for water purification. Nanomaterials 8:54
17. Gaita E, Evangelisti C, Panzarasa G (2018) A proof-of-concept portable water purification device obtained from PET bottles and a magnetite-carbon nanocomposite. Recycling 3:31. https://doi.org/10.3390/recycling3030031
18. Pompe T, Zschoche S, Herold N et al (2003) Maleic anhydride copolymers-a versatile platform for molecular biosurface engineering. Biomacromolecules 4:1072–1079. https://doi.org/10.1021/bm034071c
19. Thielemans W, Wool RP (2005) Lignin esters for use in unsaturated thermosets: lignin modification and solubility modeling. Biomacromolecules 6:1895–1905. https://doi.org/10.1021/bm0500345
20. Jiang C, He H, Yao X et al (2018) The aggregation structure regulation of lignin by chemical modification and its effect on the property of lignin/styrene–butadiene rubber composites. J Appl Polym Sci. https://doi.org/10.1002/app.45759
21. Mamdouh MN, MacKay GDM (1984) Mechanism of thermal decomposition of lignin. Wood Fiber Sci 16:441–453
22. Shao Y, Guizani C, Grosseau P et al (2017) Thermal characterization and kinetic analysis of microfibrillated cellulose/lignosulfonate blends. J Anal Appl Pyrolysis 124:25–34. https://doi.org/10.1016/j.jaap.2017.03.001
23. Jakab E, Till F, Székely T, Faix O (1991) Thermogravimetry/mass spectrometry of various lignosulfonates as well as of a kraft and acetosolv lignin. Holzforschung. https://doi.org/10.1515/hfsg.1991.45.5.355

24. Derkacheva O, Sukhov D (2008) Investigation of lignins by FTIR spectroscopy. Macromol Symp 265(1):61–68
25. Duval A, Molina-Boisseau S, Chirat C (2015) Fractionation of lignosulfonates: comparison of ultrafiltration and ethanol solubility to obtain a set of fractions with distinct properties. Holzforschung 69:127–134. https://doi.org/10.1515/hf-2014-0082
26. Shen Q, Zhang T, Zhu MF (2008) A comparison of the surface properties of lignin and sulfonated lignins by FTIR spectroscopy and wicking technique. Colloids Surf A 320:57–60. https://doi.org/10.1016/j.colsurfa.2008.01.012
27. Xiao B, Sun XF, Sun R (2001) Chemical modification of lignins with succinic anhydride in aqueous systems. Polym Degrad Stab 71:223–231. https://doi.org/10.1016/S0141-3910(00)00133-6
28. Wang F, Yang X, Zou Y (2015) The esterification of sodium lignosulfonate with maleic anhydride in water solution. Int J Polym Anal Charact 20:69–81. https://doi.org/10.1080/1023666X.2014.961117
29. Delben F, Paoletti S, Porasso RD, Benegas JC (2006) Potentiometric titrations of maleic acid copolymers in dilute aqueous solution: experimental results and theoretical interpretation. Macromol Chem Phys 207:2299–2310. https://doi.org/10.1002/macp.200600479
30. Rivas BL, Pooley SA, Pereira E et al (2006) Poly(ethylene-alt-maleic acid) as complexing reagent to separate metal ions using membrane filtration. J Appl Polym Sci 101:2057–2061. https://doi.org/10.1002/app.23794

Acknowledgements

The authors are grateful to the anonymous reviewers for their help improving the quality of this manuscript. This research did not receive any specific grant from funding agencies in the public, commercial, or not-for-profit sectors.

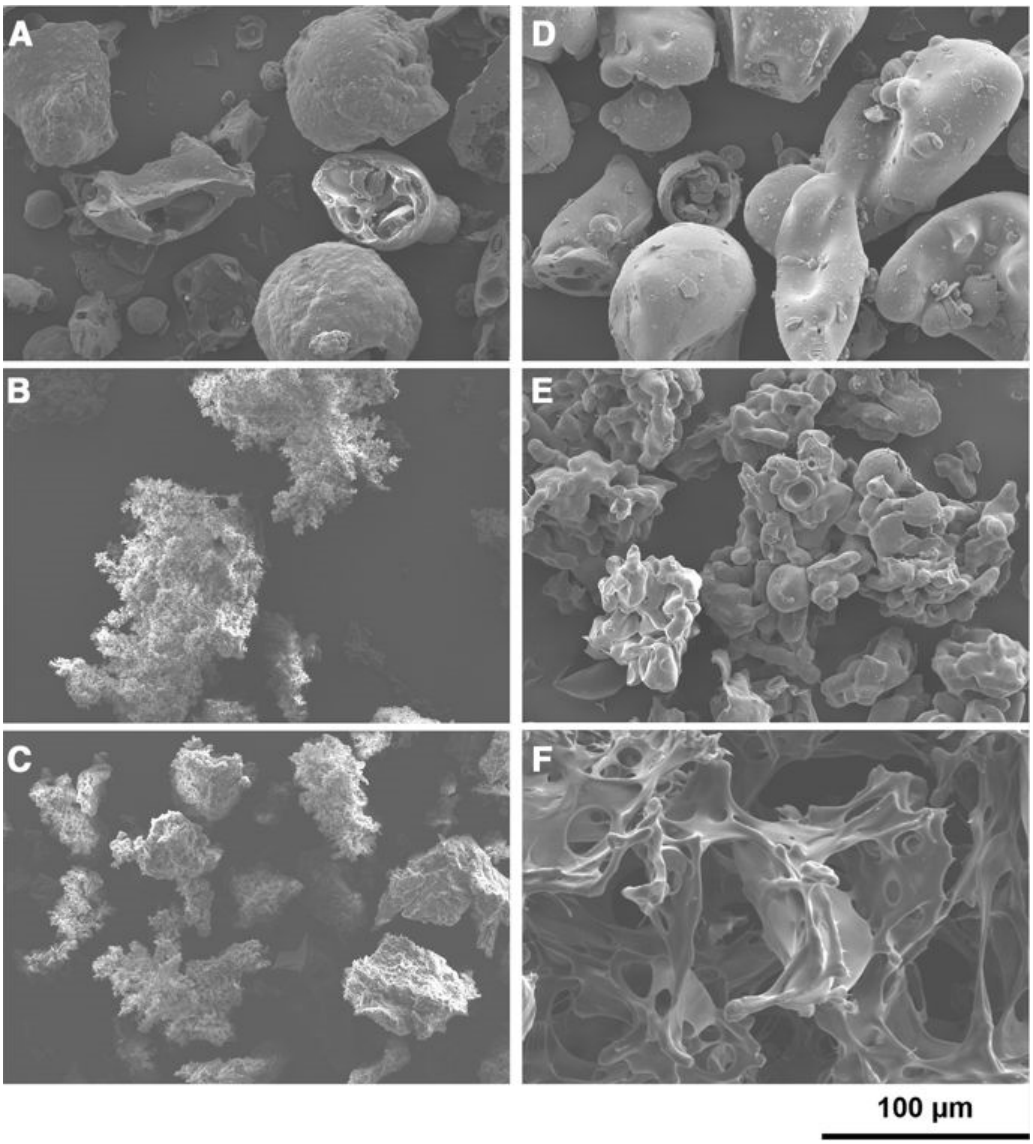

Fig. 1 Scanning electron microscopy of lignin (**a**), lignin- P(E-*alt*-MA) hybrid before (**b**) and after lyophilization (**c**), lignosulfonate (**d**), lignosul- fonate-P(E-*alt*-MA) hybrid before (**e**) and after lyophiliza- tion (**f**)

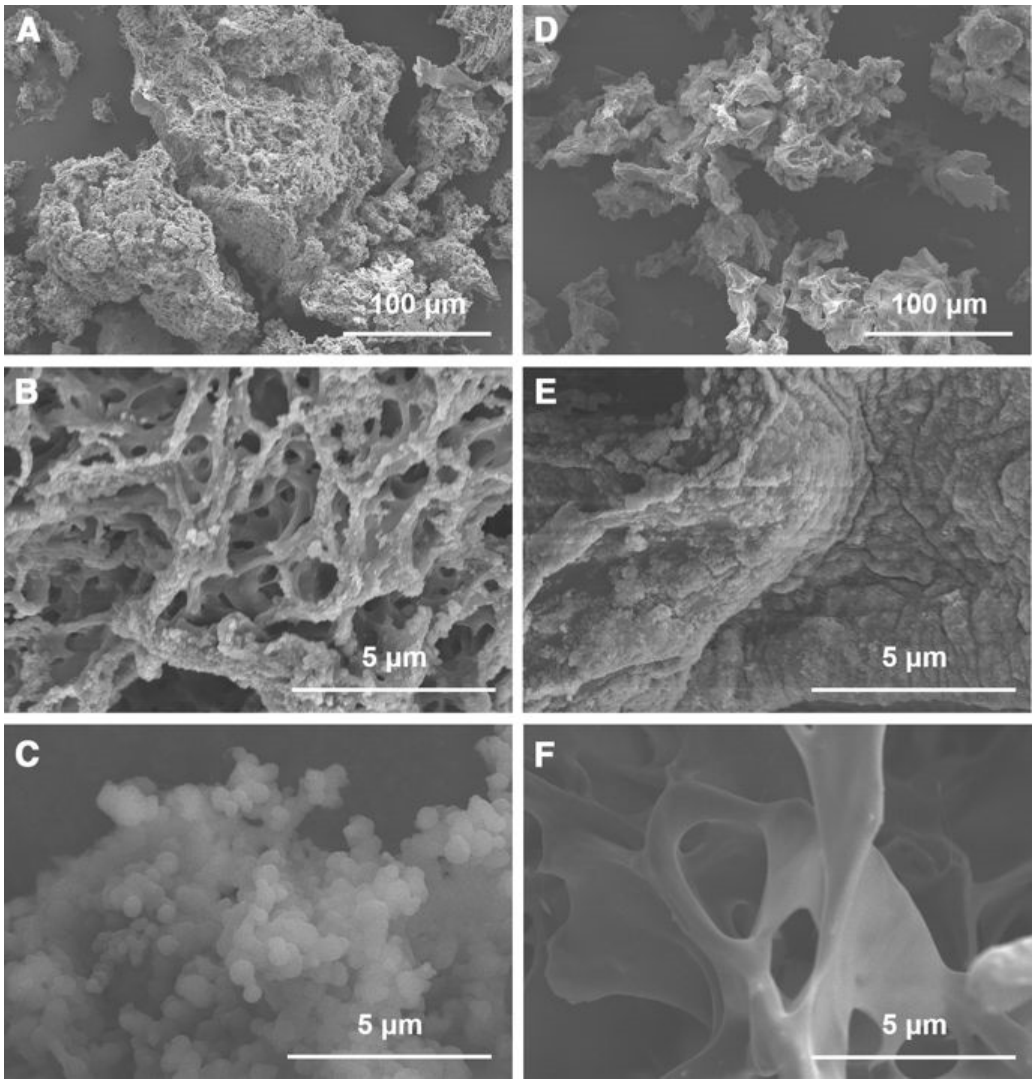

Fig. 2 SEM images of lignin- P(E-*alt*-MA) (**a, b**) and ligno-sulfonate-P(E-*alt*-MA) (**d, e**), both decorated with magnetite nanoparticles, after lyophiliza- tion. Unmodified lignin-P(E- *alt*-MA) (**c**) and lignosulfonate- P(E-*alt*-MA) (**f**) are also shown for comparison

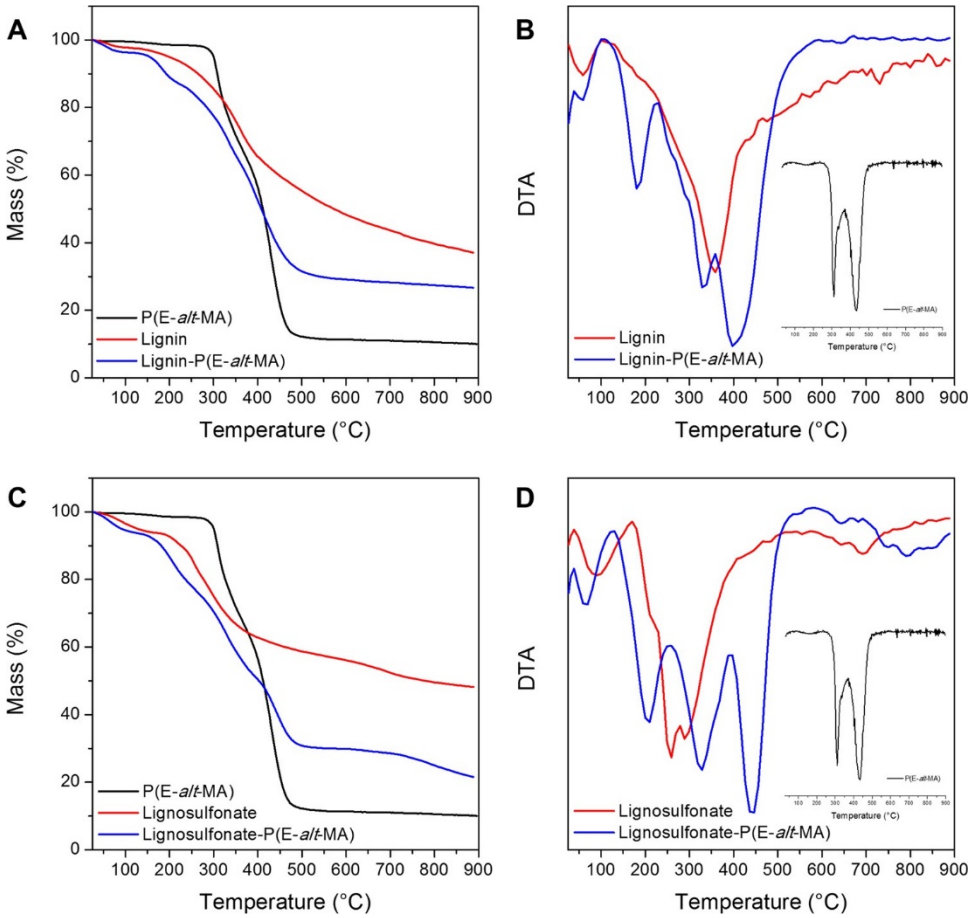

Fig. 3 TGA (**a**, **c**) and DTA (**b**, **d**) results for the raw and synthesized materials. The DTA of P(E-*alt*-MA) is represented in **b** and **d** as inset

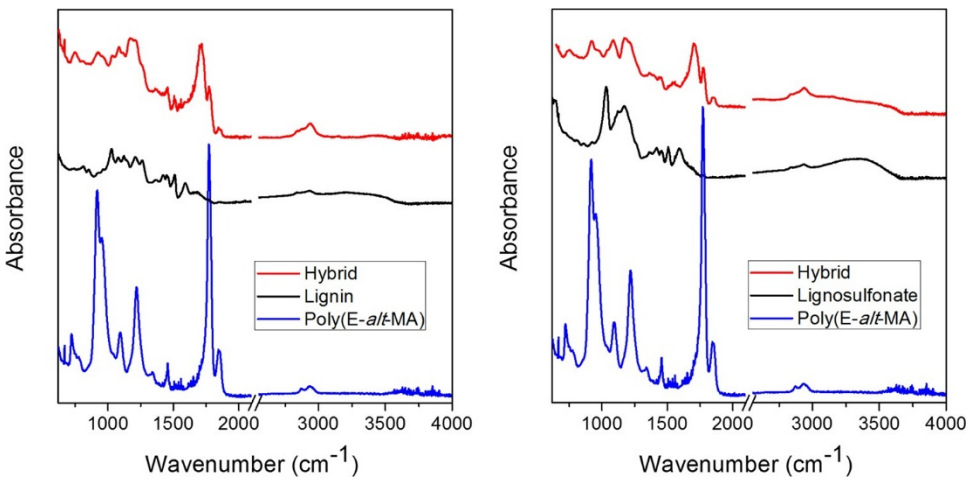

Fig. 4 FTIR spectra of the raw and synthesized materials

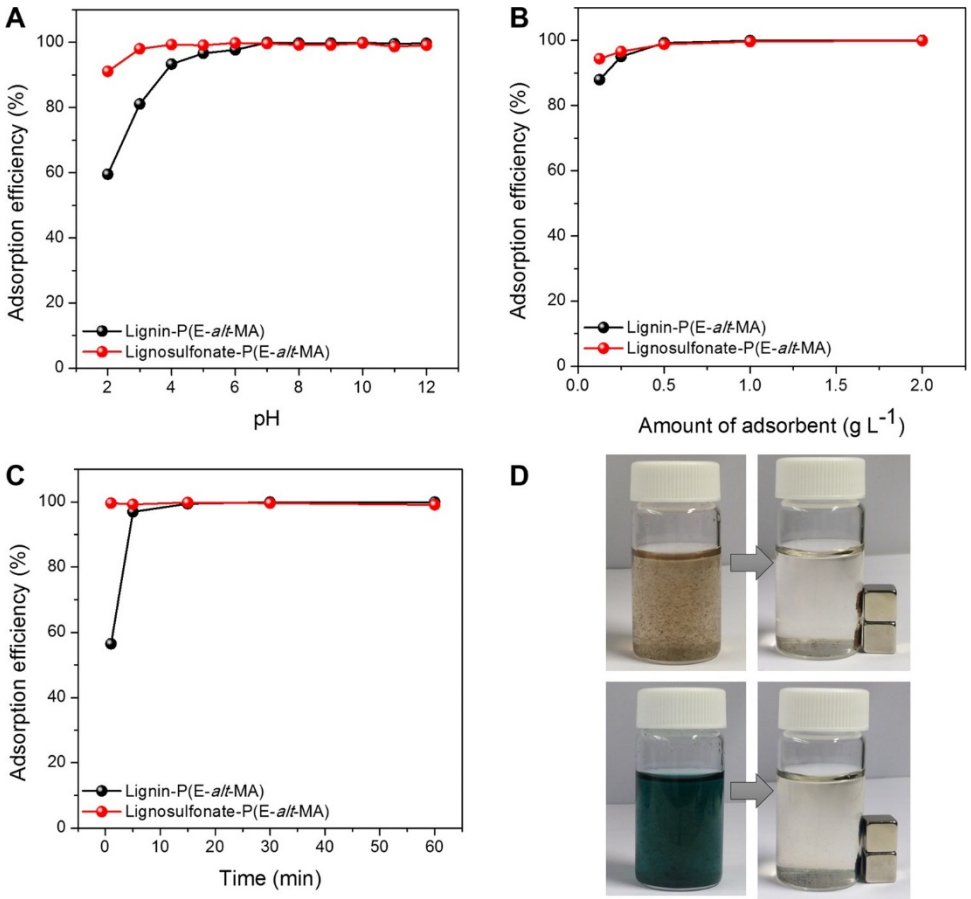

Fig. 5 **a** Effect of pH on adsorption efficiency. **b** Effect of adsorbent amount on adsorption efficiency. **c** Adsorption kinetics. **d** Demonstration of magnetic recovery for the magnetite-hybrid [conditions 0.7 g L^{-1} of lignin-P(E-*alt*-MA) magnetic hybrid; 5 mg L^{-1} MB in pH 7 phosphate buffer; adsorption time 30 min; 25 °C; 250 rpm]

Table 1 Elemental composition of the raw and synthesized materials

Sample	Elemental percentage (%)					Elemental ratios	
	C	O	S	Na	Fe	C/O	C/Fe
Lignin	68 ± 2.0	31 ± 2.1	1.6 ± 0.33	–	–	2.2	–
Lignin-P(E-*alt*-MA)	62 ± 1.1	37 ± 1.2	0.51 ± 0.36	–	–	1.7	–
Lignin-P(E-*alt*-MA)-magnetite	59 ± 2.9	39 ± 2.6	0.09 ± 0.020	–	3 ± 0.09	1.5	23
Lignosulfonate	44 ± 1.3	43 ± 0.71	6.1 ± 0.49	6.9 ± 0.15	–	1.01	–
Lignosulfonate-P(E-*alt*-MA)	55 ± 2.1	39 ± 2.4	1.2 ± 0.29	4.2 ± 0.55	–	1.4	–
Lignosulfonate-P(E-*alt*-MA)-magnetite	45 ± 2.0	42 ± 0.47	0.79 ± 0.2	–	13 ± 1.9	1.3	9.7

Table 2 Residual mass values obtained at 900 °C for the raw and synthesized materials

Sample	Residual mass (%)
P(E-*alt*-MA)	10.03
Lignin	36.76
Lignin-P(E-*alt*-MA)	26.60
Lignosulfonate	48.08
Lignosulfonate-P(E-*alt*-MA)	21.31